JOURNAL OF MATERIALS SCIENCE 32 (1997) 6357–6369

Estimation of residual stresses in SiC/Ti–15–3 composites and their relaxation during a fatigue test

J.-L. BOBET, C. MASUDA
National Research Institute for Metals, 1-2-1 Sengen, Tsukuba 305, Japan
Y. KAGAWA
University of Tokyo, Institute of Industrial Science, 7-22-1 Roppongi, Minato-ku, Tokyo 106, Japan

Residual stresses induced by cooling down from the elaboration process in SiC/Ti–15–3 composite were calculated by the finite element model using MARC and MENTAT software. An analytical model (derived from those of Eshelby and of Mikata and Taya) already used for ceramic matrix composites has also been used in this study for elementary composites. The influence of uncertainty on thermomechanical properties and also the influence of fibre packing and spacing were also studied. Then, evolution (relaxation) of the thermal residual stresses (TRS) during a fatigue test were investigated. Results show that the TRS decreased rapidly during the first cycles and then became almost constant at about one-third of their initial values.

1. Introduction

Recent efforts in the development of continuously reinforced high temperature metal matrix composites (MMCs) represent a response to the need for materials that can retain acceptable specific mechanical properties at elevated service temperature. Advanced composites show considerable promise for weight and volume critical application, for example, aircraft and space vehicles. Improvements in gas turbine engine and hypersonic vehicle technology are two potential benefits of the use of such materials. Typically, MMCs are fabricated by stacking alternate layers of thin metal matrix foils and ceramic fibres, and consolidating at elevated temperature.

When a MMC is cooled down to room temperature from the fabrication or annealing temperature, thermal residual stresses (TRS) can be induced in the composite as a result of the mismatch of the coefficients of thermal expansion (CTE) between the metal matrix and the reinforcement. The magnitude of the TRS may have a very important effect on the yield stress and fatigue strength of the MMC.

The metal matrix composite used herein in SCS-6/Ti–15–3 where Ti–15–3 is the shortened designation for Ti–15V–3Cr–3Al–3Sn and the manufacturer's designation for the silicon fibres is SCS-6 which consists of a carbon core (diameter = 30 μm) embedded in a SiC matrix (thickness = 55 μm) deposited by chemical vapour deposition and then covered by an orthotropic carbon layer (thickness = 3 μm). Ti–15–3 is currently under evaluation as a matrix material for high-temperature metal matrix composites since it can be economically cold-formed into relatively thin sheets while retaining good mechanical properties.

TRS were calculated assuming a temperature change of $-550\,^{\circ}C$; the temperature $550\,^{\circ}C$ is approximately one-half of the melting point of the Ti–15–3 matrix. It was assumed that any residual stresses that developed during fabrication of the composite would be relieved due to relaxation at temperatures greater than one half the melting point of the matrix [1].

2. Analytical model

2.1. Bulk model in composites

The general features of the differential thermal residual stress state could be seen from the formulation of Turner [2]

$$\sigma_i = K_i(\alpha_c - \alpha_i)\Delta T \quad (1)$$

where K_i was the bulk modulus of the ith phase, α_c was the volume CTE of the composite, α_i was the volume CTE of the ith phase and ΔT was the difference between the process temperature and the room temperature (this value is negative). The value of α_c was calculated from

$$\alpha_c = [\alpha_1 K_1 V_1 + \alpha_2 K_2(1 - V_1)]/[K_1 V_1 + K_2(1 - V_1)] \quad (2)$$

for a two-phase system. V_i was the volume fraction of the ith phase. Equations 1 and 2 assumed that both materials were elastic and that no cracks were present. The stresses calculated were equivalent to the hydrostatic stresses. This method was very easy and could be quickly applied to any composite material. However, it did not give the evolution of TRS on the radial

direction and so it was not possible to have information about stress distribution in the composite. This method did not give informations about radial, hoop and axial stresses; thus, it clearly appeared that applying other methods were more suitable.

2.2. Analytical cylinder model

This analytical model was based upon stress–strain equilibrium equations between the constituents under given boundary conditions of applied deformations. The set of resulting equations was then solved by a standard iterative numerical procedure.

This model was derived from that of Mikata and Taya's and had already been used for the determination of residual stresses in the case of ceramic matrix composite [3, 4].

A schematic diagram of the monocomposite showing orientation of TRS is given in Fig. 1. It was assumed that stresses were induced by a uniform change of the temperature field. This hypothesis was reasonable since end of the cool-down step was of primary importance for residual stresses determination. But the relatively slow rate of cooling and the high thermal conductivity of both materials provided additional reasons.

Hoop, radial and axial TRS components in the fibre and in the matrix were obtained from the following basic equations

$$\sigma = C\varepsilon - C\alpha\Delta T \tag{3}$$

where C referred to the stiffness tensors, ε to the strain tensor and α to the CTE tensor. ΔT was the temperature change.

The following boundary conditions were assumed (u was the radial displacement, w the axial displacement, the subscripts 1 and 2 referred to the matrix and the fibre respectively)

1. A zero radial stress at the external surface of the matrix cylinder

$$\sigma^{R(1)} = 0 \qquad \text{at } R = R(1) \tag{4}$$

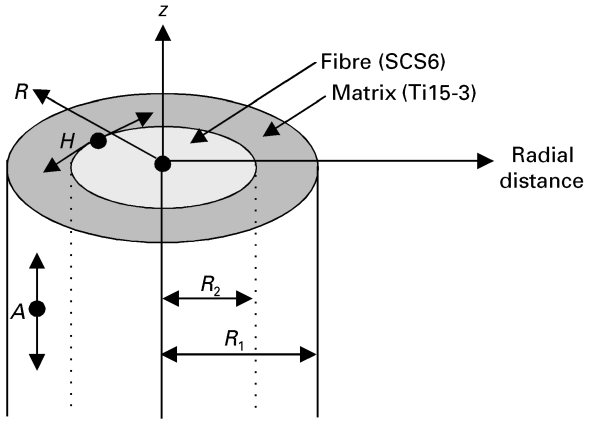

Figure 1 Schematic diagram showing the monocomposite and the stress components. R, radial stresses (σ^R); H, hoop stresses (σ^H); A, axial stresses (σ^A).

2. Continuity of displacement across the fibre–matrix interface

$$u1 = u2$$
$$w1 = w2 \qquad \text{at } R = R(2) \tag{5}$$

3. Continuity of radial stress at the fibre–matrix boundaries

$$\sigma^{R(1)} = \sigma^{R(2)} \qquad \text{at } R = R(2) \tag{6}$$

4. Sum of axial stresses in both materials was zero

$$\int_0^{R2} \sigma_l^{(2)} r\,\mathrm{d}r + \int_{R2}^{R1} \sigma_l^{(1)} r\,\mathrm{d}r = 0 \tag{7}$$

Interactive effects from the actual composite were not taken into account in this analytical analysis.

Equations of the residual stresses could be expressed as follows

$$\sigma_r = C_{11}^{(n)}\left(An - \frac{Bn}{r^2}\right) + C_{12}^{(n)}\left(An + \frac{Bn}{r^2}\right) + C_{13}^{(n)}F - \beta_1^{(n)}\Delta T \tag{8}$$

$$\sigma_\theta = C_{11}^{(n)}\left(An + \frac{Bn}{r^2}\right) + C_{12}^{(n)}\left(An - \frac{Bn}{r^2}\right) + C_{13}^{(n)}F - \beta_1^{(n)}\Delta T \tag{9}$$

$$\sigma_l = 2C_{13}^{(n)}An + C_{33}^{(n)}F - \beta_3^{(n)}\Delta T \tag{10}$$

where

$$\beta_1^{(n)} = (C_{11}^{(n)} + C_{12}^{(n)})\alpha_T^{(n)} + C_{13}^{(n)}\alpha_L^{(n)} \tag{11}$$

$$\beta_3^{(n)} = 2C_{12}^{(n)}\alpha_T^{(n)} + C_{33}^{(n)}\alpha_L^{(n)} \tag{12}$$

and $C_{xx}^{(n)}$ were the components of stiffness tensor of material n; n referred to the order of the concentric cylinder ($n = 1$ for the matrix and $n = 2$ for the fibre); E was the Young's modulus; ΔT was the temperature change ($\Delta T = -550\,^\circ\mathrm{C}$). Coefficients An, Bn and F depended on the material properties (Young's modulus, Poisson's ratio and CTE) and radial position. Closed form equations for An and Bn were determined by boundary conditions. For reasons of brevity the resulting equations for TRS will not be detailed in the present paper. They are available in reference [6].

The influence of neighbouring fibres was simulated by the presence of a third concentric cylinder with properties of the composite calculated by rules of mixtures (Section 2.5). The influence of the thickness of the surrounding composite was also studied here.

2.3. Finite Element Model Analysis of TRS

The TRS in monocomposites and usual composites were computed using the MARC and MENTAT finite element codes.

A two-dimensional axisymmetrical analysis was conducted for the monocomposite, whereas for the composite a three dimensional analysis was preferred. The volume cells were modelled by two- or three-dimensional isoparametric elements as indicated in Table I. The meshes constructed for the analysis are exemplified in Figs 2 and 3 which show those meshes

TABLE I Data on the meshes constructed for the finite element analyses

	Numbers of elements	Element type	Type of analysis
Monocomposites			
without SC	675	8 nodes	2D
with SC	1050	rectangles	axisymmetrical
Composites	12 352	27 nodes cubes 10 nodes tetrahedrons 15 nodes triangular prisms	3D

SC = surrounding composite.

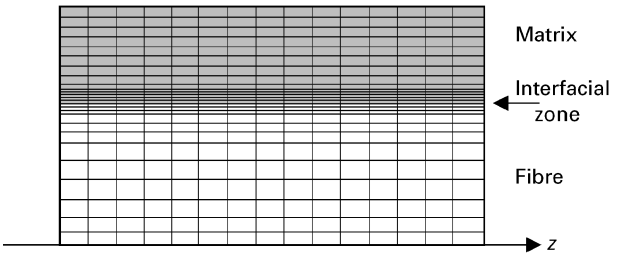

Figure 2 Mesh used for the FEM calculation of residual stresses in the monocomposite without surrounding composite (z is the symmetry axis).

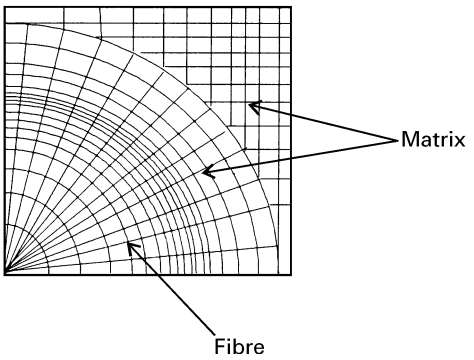

Figure 3 Example of mesh used for the FEM analysis of the composite.

constructed for the monocomposite and for the unit cell of composite.

The boundary condition for this problem were straightforward. They should be such that the symmetry was retained, i.e. the symmetry planes should remain in-plane and the angles between planes should be retained. Therefore all the nodes at the symmetry surfaces were constrained to have the same normal displacement.

Various fibre packing arrangements including cubic (Fig. 4) and hexagonal patterns (Fig. 5) were examined. Fibres were either uniformly distributed (Figs 4 and 5) or not (in contact, for example, as shown in Fig. 6). Influence of the distance between fibres were also studied here. A cubic packing arrangement only was considered for this latter case because it was assumed to be more representative of the situation in reality and also because it was observed that fibre packing arrangement exerted a limited influence on TRS distributions. The unit cell repeated itself

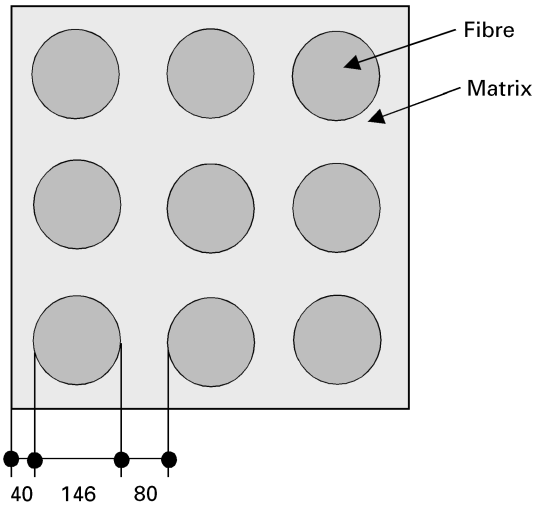

Figure 4 Example of FEM unit cell model for the analysis of TRS in composite with a uniform distribution of fibres (cubic fibre packing arrangement). Dimension in μm.

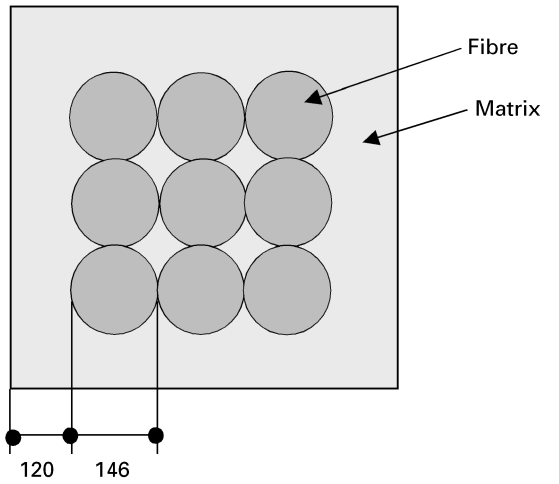

Figure 5 Example of FEM unit cell model for the analysis of TRS in composite with fibres in contact (cubic fibre packing arrangement). Dimensions in μm.

throughout the composite when the fibres were assumed to be identically packed throughout the entire composite. The residual stresses in the composite could be found by an analysis of this representative volume cell.

The one-unit fibre model was vertically stacked to simulate a four-ply model and an eight-ply model. This arrangement of the model geometry resulted in

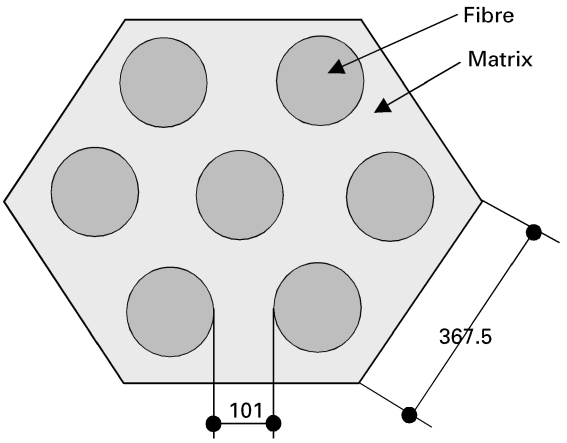

Figure 6 Example of FEM unit cell model for the analysis of TRS in composite with fibres in contact (hexagonal fibre packing arrangement). Dimensions in μm.

simulating a four-ply and eight-ply unidirectional composites. As demonstrated later in the Results and Discussion section, these multi-ply models show that the underlying plies have significant effects on the surface residual stresses.

Two thermal loading states were prescribed. The unit cells were assumed initially at a uniform temperature of 558 °C (state 1). Then in state 2, the temperatures were uniformly set to 20 °C by steps of 50 °C (last step of 38 °C only).

2.4. Evolution of TRS during a fatigue test

In this study, the simplified method of Zarka and Casier [10] was used. Only the matrix far from the fibre was taken into account and the behaviour was then assumed to be that of a metal compound. This hypothesis clearly simplified the phenomenon, eliminating the effects of softening or hardening. However, in order to know the trend of the evolution of TRS, this method could be used. When a structure was loaded in cyclic plasticity (it was the case of the relaxation of residual stresses which come from cyclic microdeformations), this method did not lead to the exact solution, but it was possible to predict a reasonable indication of the stabilized state and also the behaviour to stabilized cycle: elastic or plastic shakedown (Fig. 7).

The key point of Zarka and Casier's method consisted of the introduction into the calculations of the stresses and deformations, a transformed variables field. It was determined from the stress field by the relations

$$\alpha' = \alpha - \mathrm{dev}\,\rho = \alpha - s - s^{el} \tag{13}$$

where α' = transformed internal parameter; α = internal parameter related to the cinematic *ecrouissage*; $\alpha = C\varepsilon^p$ where ε^p is the tensor of plastic deformations; ρ = tensor of residual stresses; s = deviator of tensor of global stresses; s^{el} = deviator of tensor of elastic stresses; $C = \frac{2}{3}H$ where H is cyclic *ecrouissage* modulus of the material. Then, the Mises plastic criterion which governs the evolution of plastic deformations could be rewritten as follows

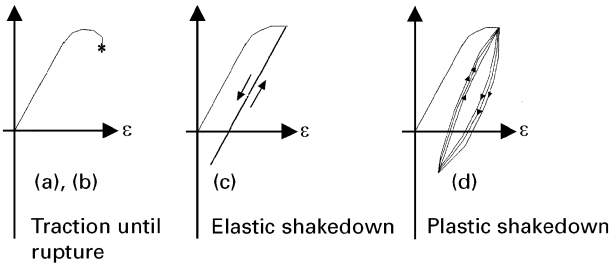

Figure 7 Graphical representation of different responses of a material under cyclic loading: (a) purely elastic response; (b) fracture during the first cycle; (c) elastic shakedown; (d) plastic shakedown.

$$\tfrac{3}{2}(s - \alpha)^T(s - \alpha) \leqslant \sigma_0^2 \tag{14}$$

where σ_0 was the true elastic limit (limit of cyclic elasticity). From Equation 13 this becomes

$$s - \alpha = s^{el} - \alpha' \tag{15}$$

then, the new criterion of plasticity is

$$\tfrac{3}{2}(s^{el} - \alpha')^T(s^{el} - \alpha') \leqslant \sigma_0^2 \tag{16}$$

This relation determined, in the three dimensional space of α', a convex domain, limited by a surface which was constituted by the representative points of the stress states which correspond to the elastic limit of the material. This surface was a sphere (radius = σ_0 = true elastic limit and centre = s^{el}).

In the space of the transformed variables, the interpretation of the plastic criterion was as follows: if the state of non-linearity (plasticity) of the material was locally defined by the tensor of parameters α', the representative point of the stress state had to stay always in or at the surface of the sphere (radius = σ_0 and centre = s^{el}).

When the load varied as a function of time, the position and size of the convex domain also varied (Fig. 8), but still only dependent on parameters which could be determined by elastic calculations.

When the studied structure was subject to cyclic loading ($F_{min} < F < F_{max}$), the representative point of the stress state moves to and from the two convex domains (C_{min} and C_{max} as shown in Fig. 9).

When the limit of elasticity remained constant, the sphere radius was still constant ($\sigma_{0\,min} = \sigma_{0\,max} = \sigma_0$). On the other hand, in this hypothesis, the necessary and sufficient condition for elastic shakedown (and this stabilization of the level and state of residual stress for example), for Zarka and Casier's method, was that the intersection between two spheres was non-zero (Fig. 9).

From a mathematical point of view, this condition could be written as

$$[\tfrac{3}{2}(\Delta S^{el})^T(\Delta S^{el})]^{1/2} \leqslant 2\sigma_0 \tag{17}$$

where:

$$\Delta S^{el} = S^{el}_{max} - S^{el}_{min} \tag{18}$$

If this condition was not satisfied, then, there was plastic shakedown. The representative point of the elastic shakedown state was obviously in the intersection area shown on Fig. 9. So, the method consisted of

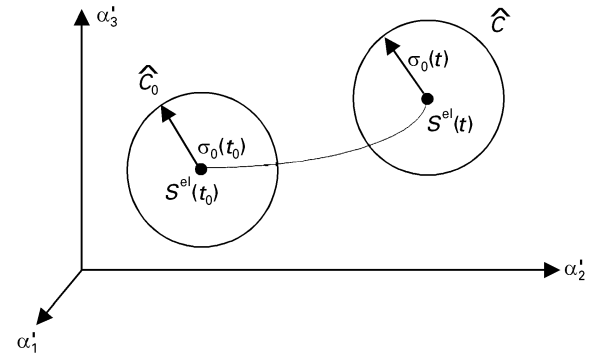

Figure 8 Graphical representation of the evolution when the loading condition changes between initial time t_0 and t.

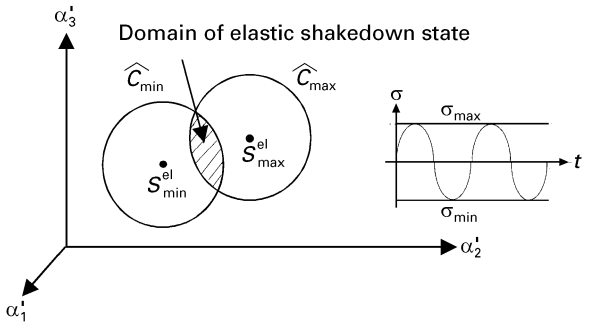

Figure 9 Graphical representation of elastic shakedown condition in the space of the transformed internal parameter α.

checking (by calculation) the elastic shakedown condition from (a) the mechanical and cyclic properties of the material (obtained from Equation 11), (b) the initial thermal residual stresses (calculated as shown in Sections 2.2 and 2.3) and applied loading.

Reference [10] gives more detail about this method and explains how to obtain an approximation of the adapted (elastic shakedown) stress state. The major interest in this method is to provide an approximate solution using only a few elastic calculations.

2.5. Material properties

In the present work the matrix material was assumed to be isotropic. The properties of the fibre were assumed to be isotropic or orthotropic as shown in Table III. Then, effect of temperature dependence are assumed for both fibre and matrix (Table II). The properties of the surrounding composites were calculated by two different rules of mixtures (ROM). The first, easier one, is called ROM 1

$$P_c = P_f V_f + P_m(1 - V_f) \tag{19}$$

where P_c, P_f and P_m were the properties of the composite, the fibre and the matrix respectively. V_f was the volume fraction of the fibre.

The second mixture rule, called ROM 2, was used to simulate orthotropic properties for the surrounding composite. It is expressed as follows

$$E_{c,a} = V_f E_f + (1 - V_f) E_m \tag{20}$$

$$E_{c,r} = E_m E_f / [V_f E_m + (1 - V_f) E_f] \tag{21}$$

TABLE II Temperature-dependent constituent properties for SCS-6/Ti–15–3

Elastic properties			
Temperature (°C)	E (GPa)	ν (C^{-1})	α (10^6)
Ti–15–3 matrix (as fabricated)			
21.1	92.39	0.36	8.208
204	92.39	0.36	8.946
427	84.81	0.36	9.504
538	58.61	0.36	9.756
SCS-6 Fibre			
21.1	393	0.25	3.564
93.3	390	0.25	3.564
204	386	0.25	3.618
316	382	0.25	3.726
427	378	0.25	3.906
538	374	0.25	4.068
649	370	0.25	4.266
760	365	0.25	4.41
871	361	0.25	4.572
1093	354	0.25	–

TABLE III Thermomechanical properties of the constituents used in the calculation when no dependence against temperature was assumed

	E_L (GPa)	E_T (GPa)	ν	α_L ($\times 10^6$)	α_R ($\times 10^6$)
Fibre					
SCS-6 [8]	390	390	0.25	3.90	3.90
SCS-6 [9]	407	407	0.15	5.50	2.63
Matrix					
Ti–15–3 [8]	92	92	0.35	9.72	9.72

As the Poisson's ratios of the two materials are not too different, the coefficient of thermal expansion is expressed as follows

$$\alpha_{c,a} = [V_f E_f \alpha_f + (1 - V_f) E_m \alpha_m] / [V_f E_f + (1 - V_f) E_m] \tag{22}$$

$$\alpha_{c,r} = V_f(1 + \nu_f)\alpha_f + (1 - V_f)(1 + \nu_m)\alpha_m - \nu_c \alpha_{c,a} \tag{23}$$

The thermal and mechanical properties assumed for the constituents are given in Tables II and III.

As many different properties for the fibre and the matrix could be found in the literature, variations of CTE and Young's modulus were also investigated in the range 1 to 15×10^{-6} for the CTE and 10 to 600 GPa for Young's modulus. This suggested which properties had a major effect on TRS.

3. Results

3.1. Thermal residual stress calculations in monocomposites

Yield of the matrix was determined by comparing the von Mises equivalent stress calculated at room temperature with the room temperature yield stress (689.5 MPa [5]). When the von Mises equivalent stress was greater than or equal to the yield stress, the

yield of the matrix was assumed. The von Mises equivalent stress σ_{vm} is defined as follows

$$\sigma_{vm} = [\sigma_x^2 + \alpha_y^2 + \sigma_z^2 - \sigma_x\sigma_y - \sigma_y\sigma_z - \sigma_z\sigma_x + 3(\tau_{xy}^2 + \tau_{yz}^2 + \tau_{zx}^2)]^{1/2}$$

No yield of the matrix was calculated to occur during the fabrication process; thus, only results for the linear analyses were presented.

The three normal stress components, σ_r, σ_θ and σ_l can be related to different types of damage in the form of cracking. The radial stress component, σ_r, controls interfacial or circumferential cracking. The most common example of this type of cracking is fibre-matrix debonding. The hoop stress component, σ_θ, controls radial cracking. The longitudinal or axial stress component, σ_l, governs cracking perpendicular to the fibre direction.

The Turner equations (Section 2.1) led to the following results in the case of SiC/Ti–15–3 composite: $\alpha_c = 5.74\times10^{-6}\,^\circ C^{-1}\sigma_f = -380$ MPa, $\alpha_m = 179$ MPa.

As previously noted, these results were not sufficient because there was no information about stresses distribution and also about stress direction (radial, hoop or axial). However, it appeared that the matrix was in tension and fibre in compression. The calculated TRS were lower than the room temperature yield stress so there was no matrix yield.

Using the analytical model and also the finite element model (FEM) analysis, it was possible to determine the distribution of the TRS along the radial direction. Furthermore, using FEM, it was possible to get information about stresses in the interfacial area. Both calculations led to the same results but the analytical solution was faster than FEM so the first one was used to predict the evolution of stresses and then, in some cases, the FEM analysis was used to get information on the stress distribution near the interface. The following results were obtained with both methods.

3.1.1. Influence of mechanical properties

Most authors report and use the same data for calculations of TRS in SiC/Ti–15–3 composite. These appear in Table III [8] and constitute the basic results, so we compared all the data to those obtained using this data set. Typical results were shown in Fig. 10. Results were similar to those already reported by several authors [8, 13, 14]. The axial stresses in the matrix were about 220 MPa (tensile). The radial stresses were compressive and about -120 MPa. The hoop stresses were compressive in the fibre (-150 MPa) and tensile in the matrix ($+240$ MPa).

3.1.1.1. Orthotropy of the fibre. A few authors report that the fibre is strongly anisotropic (as SiC is elaborated by chemical vapour deposition, a texture of SiC should exist which leads to transverse isotropic properties of the fibre) and they propose to use a transverse isotropic set of mechanical properties [9] (Table III). Results obtained using this set are shown in Fig. 11.

By comparison with Fig. 10, it appears that:

1. The sign of the TRS is the same in both case which means that tensile stresses are still tensile and compressive ones are still compressive;
2. The absolute values of axial stresses decreases by about 15% or so, the compressive stresses in the fibre become less compressive and the tensile stresses in the matrix become less tensile;
3. The absolute values of radial and hoop stresses increase by about 10% or so, the radial stresses in both fibre and matrix become less compressive and the hoop stresses in the matrix become more tensile.

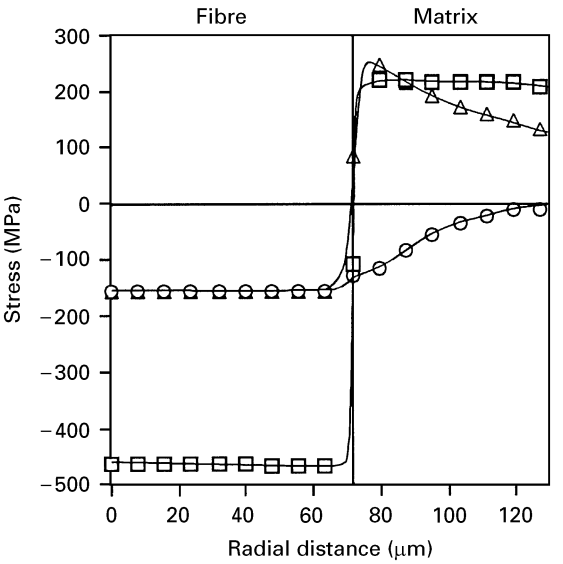

Figure 10 Thermal residual stress distribution along radial distance in a monocomposite determined using analytical and FEM models. □ axial stress; ○ radial stress; △ hoop stress.

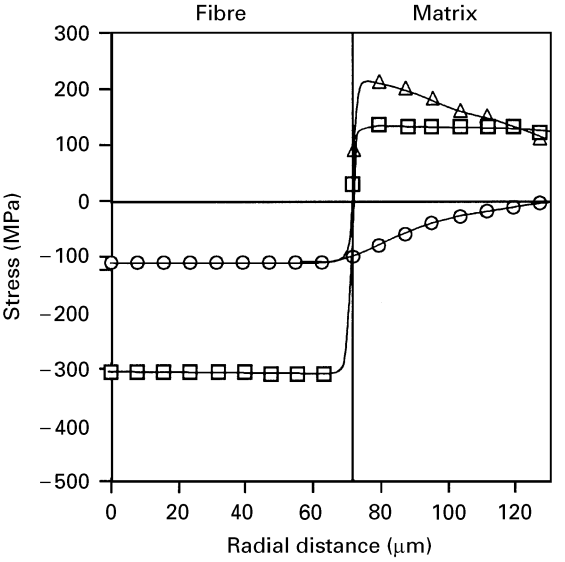

Figure 11 Thermal residual stress distribution along radial distance in a monocomposite determined using analytical and FEM models. The fibre is assumed to exhibit a transverse anisotropy as reported by Kagawa [9]. □ axial stress; ○ radial stress; △ hoop stress.

However, it is clearly shown in Figs 10 and 11 that taking into account the anisotropy of the fibre did not greatly affect the TRS results.

3.1.1.2. Temperature dependence. More and more authors report thermomechanical properties for both materials (fibre and matrix) as dependent on temperature. The data reported by these authors are summarized in Table II. The results shown in Fig. 12 are obtained by FEM analysis.

By comparison with Fig. 10, it appears that:

1. The axial stresses decrease in absolute value by about 30%, the tensile stresses in the matrix become less tensile and the compressive ones in the fibre become less compressive;
2. The radial stresses decrease in absolute value also by about 30%, compressive stresses in the fibre and in the matrix become less compressive;
3. The hoop stresses decrease in the matrix and become less tensile.

Generally speaking, when the properties depend on temperature, the level of TRS decreased by approximately 30% because the Young's modulus and the CTE of both materials (i.e. fibre and matrix) were, respectively, lower and higher when temperature increased. Thus, when no dependence upon temperature was assumed, the higher Young's modulus and higher CTE were taken into account so that the level of the calculated TRS were higher. However, it also appeared that there was no change of sign.

3.1.1.3. Variations of the mechanical properties. As it has been shown before there was a large uncertainty in the mechanical properties of both material and the calculated stresses could be affected by this uncertainty. It appeared to be of major interest to know which were the significant data (Young's modulus or coefficient of thermal expansion, and, fibre or matrix data). In order to get information about this, calculations were done assuming a large range of properties. To know the influence of the uncertainty on fibre Young's modulus, all the other properties were taken as constant and the Young's modulus was varied from 10 to 600 GPa. Two different representations were used: (i) stresses versus Young's modulus of the fibre (or the studied property) and (ii) normalized stresses versus normalized property as explained below.

The normalized stresses, σ_n, were (in the case of fibre Young's modulus variations): $\sigma_n = (\sigma_x - \sigma_{390})/\sigma_{390}$. Where σ_x was the stress calculated with Young's modulus equal x and σ_{390} the stress calculated with Young's modulus equal 390 GPa.

In the same condition the normalized property was: $E_n = (X - 390)/390$.

This last representation permitted us to determine a slope and this slope was characteristic of the influence of the parameter's uncertainty. When the slope was close to, or higher than, one then the incidence of

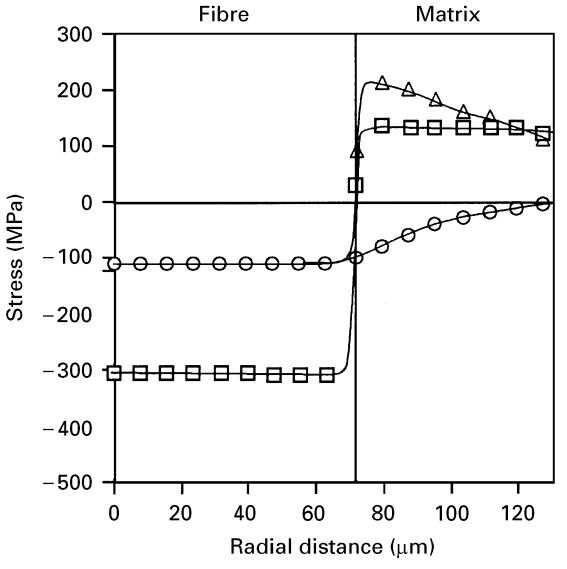

Figure 12 Thermal residual stress distribution along radial distance in a monocomposite determined using analytical and FEM models. The thermomechanical properties of both materials depend on temperature as reported by Kagawa [9]. □ axial stress; ○ radial stress; △ hoop stress.

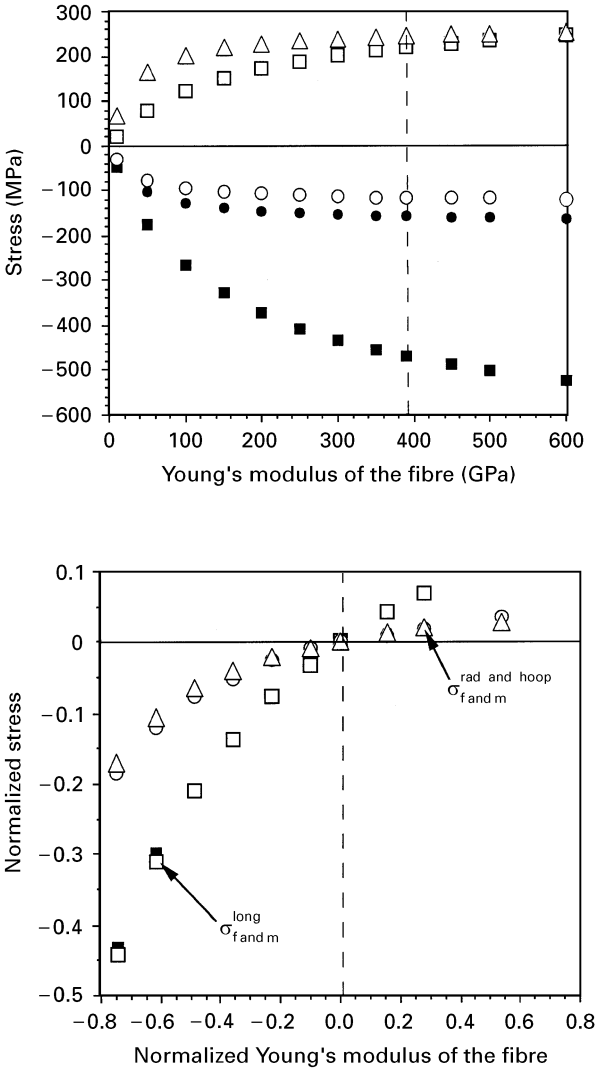

Figure 13 Thermal residual stress at 5 μm of the fibre–matrix interface in the fibre and in the matrix as a function of the fibre Young's modulus. f, fibre; m, matrix; long, longitudinal; rad, radial; ■ σ_f^{long}; ● σ_f^{rad}; □ σ_m^{long}; ○ σ_m^{rad}; △ σ_m^{hoop}.

the parameter's uncertainty was very high and reciprocally when the value of the slope was less than 0.5 it meant than the uncertainty on the studied parameter was very low.

The "normal values" were those reported in Table III and reference [8]. The influence of Young's modulus and CTE of both fibre and matrix were investigated. Results are shown in Figs 13 to 16.

Fig. 13 shows the influence of the uncertainty on fibre Young's modulus. From this figure, it appears that the fibre Young's modulus does not greatly affect the TRS level. The axial stresses were the more sensitive but an uncertainty of 100 GPa led to a variation of less than 30 MPa on stress level. It is also important to note that taking into account the surrounding composite increases this effect and it was possible to inverse the sign of the radial stresses (compressive for lower values of E_f and tensile for higher values). The calculated slope on Fig. 13b was about $+0.25$ (maximum) implying that E_f has a very low effect on stress calculations.

Fig. 14 shows the influence of the uncertainty on fibre CTE. From this figure, it appears that the fibre CTE more strongly affects the TRS level than E_f. An uncertainty of 10^{-6} on α_f causes a variation of nearly 30% in the stress level (all the stresses are so affected). The calculated slope in Fig. 14b is about -0.70 (maximum) implying that α_f has a rather high effect on stress calculations. The negative slope implies that increasing α_f causes a decrease in absolute values of the stresses in both materials. The presence of the surrounding composite did not change the behaviour. Uncertainty in the CTE of the fibre significantly affects the axial TRS acting in the fibre whereas influence on the radial TRS in both fibre and matrix was limited.

Fig. 15 shows the influence of the uncertainty on matrix Young's modulus. From this figure, it appears that the matrix Young's modulus greatly affects the stress level (more than E_f and at least as much as α_f). The calculated slope in Fig. 15b varies from $+0.60$ to $+0.95$. These values close to 1 signify strong influence of E_m on TRS calculation. A variation of only 10 GPa on E_m led to a variation of 30 to 50 MPa on TRS results. The presence of the surrounding composite did not change the behaviour and the slope remained constant.

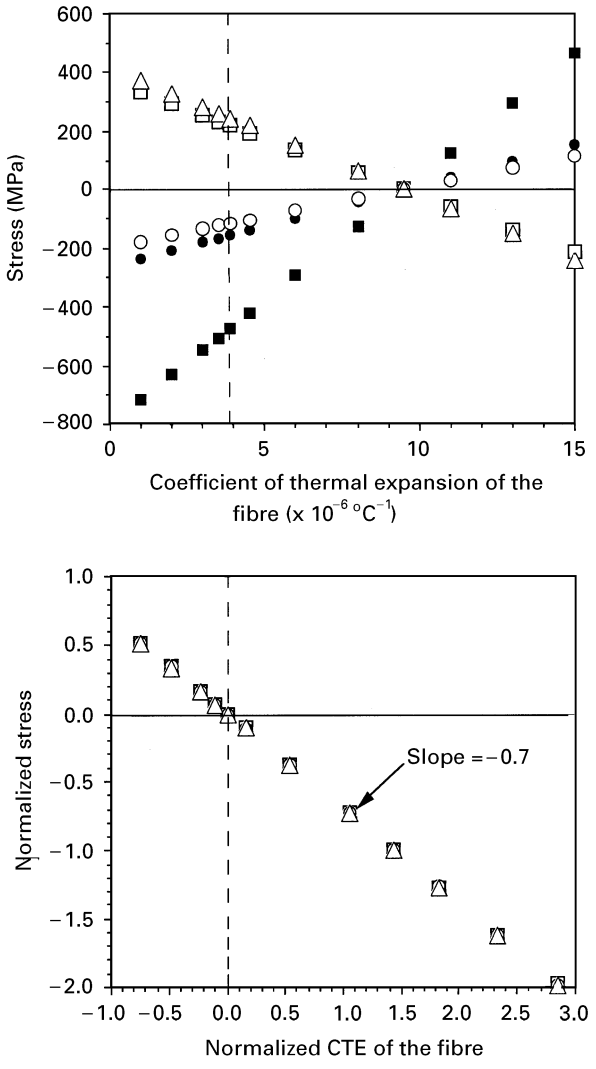

Figure 14 Thermal residual stress at 5 μm of the fibre–matrix interface in the fibre and in the matrix as a function of the fibre CTE. f, fibre; m, matrix; long, longitudinal; rad, radial; ■ σ_f^{long}; ● σ_f^{rad}; □ σ_m^{long}; ○ σ_m^{rad}; △ σ_m^{hoop}.

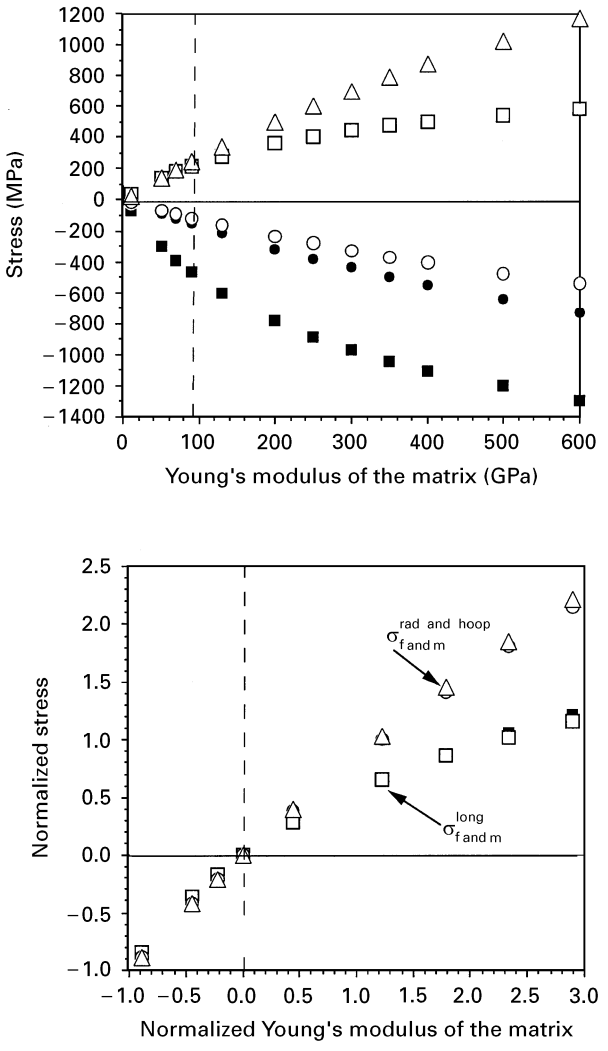

Figure 15 Thermal residual stress at 5 μm of the fibre–matrix interface in the fibre and in the matrix as a function of the matrix Young's modulus. f, fibre; m, matrix; long, longitudinal; rad, radial; ■ σ_f^{long}; ● σ_f^{rad}; □ σ_m^{long}; ○ σ_m^{rad}; △ σ_m^{hoop}.

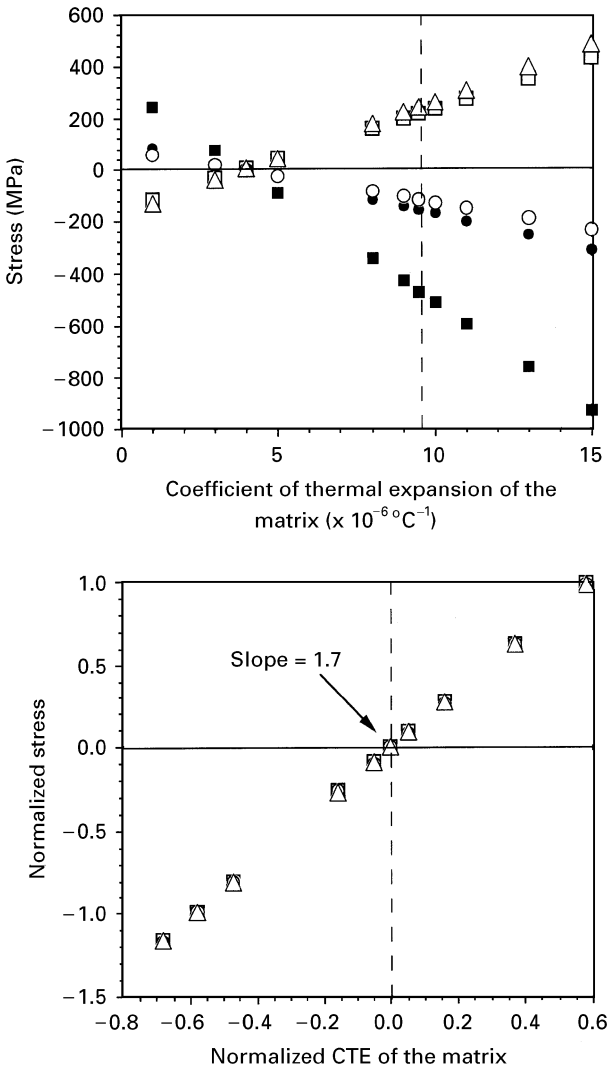

Figure 16 Thermal residual stress at 5 μm of the fibre–matrix interface in the fibre and in the matrix as a function of the matrix CTE. f, fibre; m, matrix; long, longitudinal; rad, radial; ■ σ_f^{long}; ● σ_f^{rad}; □ σ_m^{long}; ○ σ_m^{rad}; △ σ_m^{hoop}.

Fig. 16 shows the influence of uncertainty on matrix CTE. As logically expected from the previous results, matrix CTE played the major role for TRS calculations. The calculated slope in Fig. 16b is higher than 1 (+ 1.70). A variation of only 10^{-6} on α_m led to a variation of 20 to 60 MPa on TRS results (the variations were about 20%). The presence of the surrounding composite increases slightly the phenomenon (slope = 1.85).

From these results, it clearly appears that the thermomechanical properties of the matrix must be known with good accuracy to allow comparison of experimental data and calculated TRS results.

3.1.2. Influence of matrix thickness

In a real composite, the distance between two fibres could vary so that the volume fraction of the matrix surrounding each fibre was not constant. This point will be discussed more precisely in Section 3.2 but a quick approach is made here.

Calculations were done over a large range of matrix volume fractions (from 0.1 to 0.9) with properties reported in Table III and reference [8] (however, the calculations done with properties from reference [9] and/or from Table II led to the same results). TRS calculated near the interface (at 3 μm from it) in both materials were plotted as a function of matrix volume fraction in Fig. 17.

The effects of matrix thickness upon TRS were in agreement with logical expectations. Results show that TRS decreases when the matrix is thicker. It was important to note that the fourth boundary condition of the analytical model presented in Section 2.2 permits prediction of this result. The most affected stresses were the axial ones but a variation of about 10 μm (about 10% of matrix volume fraction) led to a variation of the axial stresses of only 10 to 20 MPa. It is also important to note that the values are more sensitive in the fibre than in the matrix (Fig. 17a and 17b). However, TRS dependence upon matrix thickness is not significant provided that the volume fraction of matrix remains within reasonable bounds, far from the limit of 1.

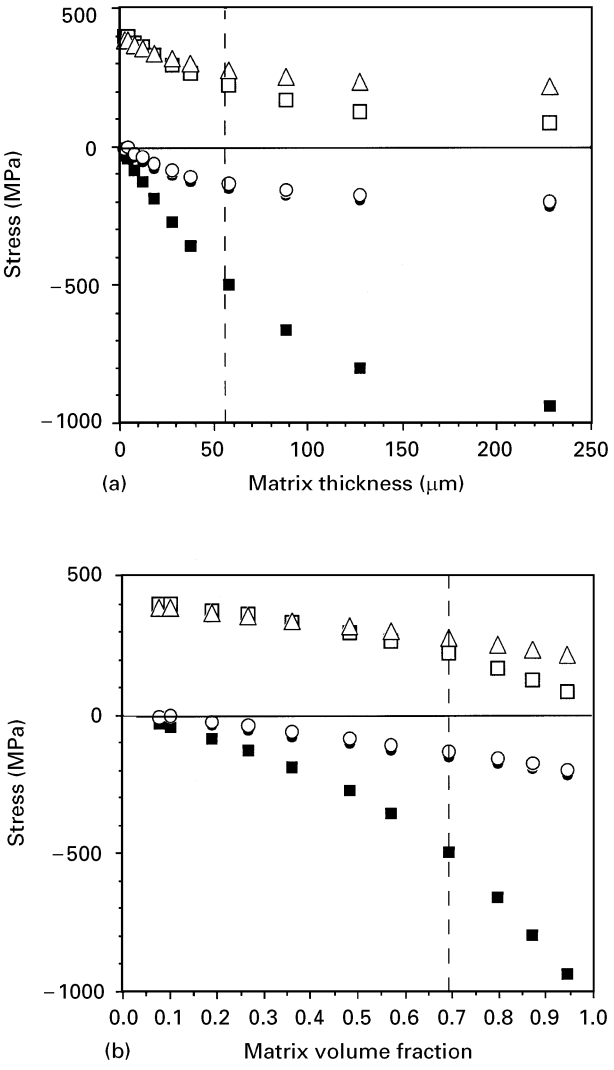

Figure 17 Variation of TRS at 3 μm of the fibre–matrix interface in both materials as a function of (a) matrix thickness and (b) matrix volume fraction. f, fibre; m, matrix; long, longitudinal; rad, radial; ■ σ_f^{long}; ● σ_f^{rad}; □ σ_m^{long}; ○ σ_m^{rad}; △ σ_m^{hoop}.

3.1.3. Influence of the surrounding composite

Many authors, in order to take into account the whole composite, use a surrounding composite (SC) element with the properties of the composite and which should simulate the neighbouring fibre. In a previous study, it has been shown that this could be a suitable approach when using only analytical model but it is better to use a "true composite", modelled by FEM. However, the SC method allowed very quick results which could be compared with the results obtained on the "true composite" with FEM analysis.

The model developed by Mikata and Taya [15] assumed an infinite thickness for the SC element but other models and other FEM calculations took thicknesses of about 100 to 2000 μm. So it should be of major interest to study the effect of the SC thickness. Furthermore, the properties of the SC could be calculated by the rules of mixtures presented in Section 2.5 or taken from the literature. The literature data for the composite were very poor so that most authors used rules of mixtures to calculate the properties of the SC. As shown in Section 2.5, there are two different rules of mixtures used depending on the nature of the SC (orthotrope or isotrope) so the calculations were done using both rules.

3.1.3.1. Thickness of the SC. The presented results are those obtained using the first rule of mixture, but the trends were similar using both rules. Fig. 18 shows the evolution of TRS as a function of SC thickness. The following interesting features should be highlighted:

1. A minimum thickness of the SC was highlighted and it was about 500 μm. Beyond this critical value, there is no more variation of the stress level in both materials and in the three directions;
2. The presence of the SC increases the level of all the stresses in both materials;
3. The axial and hoop stresses in the matrix increase and becomes more tensile in the presence of the SC;
4. The axial stresses in the fibre decrease and become less compressive, implying that the SC supports a part of axial stresses (and the axial stresses in the SC were compressive as in the fibre);
5. Radial stresses in both materials become tensile when the SC is thicker. Transition from compressive to tensile stresses is at a critical SC thickness of about 120 μm (less than the critical thickness required to get no more variation of the stress level).

With regard to point 1 it was shown that a minimum thickness of the SC is required to get results which are not influenced by the thickness of the SC and from point 5 it is shown that the radial stresses change sign (compressive to tensile stresses). As a first step, these results suggest that the radial stresses in the "true composite" should be tensile so that the fibre–matrix debonding was favoured by the presence of the neighbouring fibres. But, as has been shown in previous studies [3, 4, 6], taking into account the SC (to simulate the neighbouring fibres) was not the best way because it could lead to different results depending only on the chosen thickness of the SC. So, before making conclusions, it is better to study the values from FEM analysis. However, these results show that the axial stresses in the matrix increase in the presence of SC and also show that a minimum thickness of 500 μm for the SC is required.

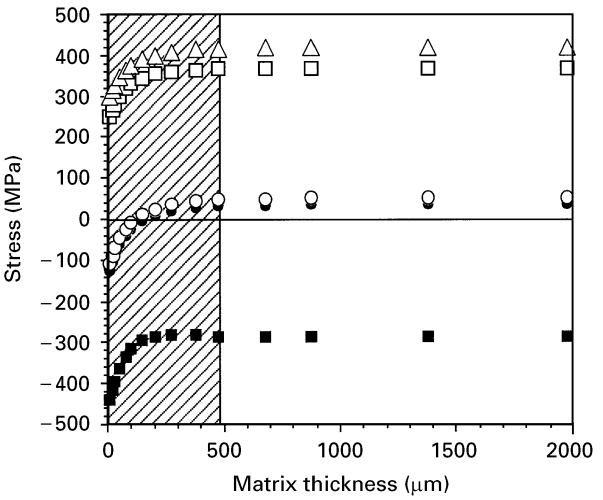

Figure 18 Variation of TRS at 3 μm of the fibre–matrix interface in both materials as a function of the surrounding composite thickness. f, fibre; m, matrix; long, longitudinal; rad, radial; ■ σ_m^{long}; ● σ_f^{rad}; □ σ_m^{long}; ○ σ_m^{rad}; △ σ_m^{hoop}.

3.1.3.2. Rules of mixtures. Using ROM2 takes into account the orthotropy of the SC. The same trends as those previously reported were observed using ROM2 (rather than ROM1). The major difference was for radial stresses which remain compressive despite increasing the SC thickness. Furthermore, the tensile axial stresses in the matrix decreased (by about 30%) and the axial stresses in the fibre increased in absolute value (becoming more compressive). Examples of calculated TRS are given in Table IV.

From these results and those previously reported about the SC thickness it clearly appears that using a SC to simulate the presence of the neighbouring fibre was not the best way, as many parameters (SC thickness, ROM used to determine the properties of the SC) could influence the results. FEM analysis appears to be the best way to estimate the effects of the neighbouring fibres in the "true composite".

3.2. Thermal residual stress calculations in "true composite"

The relevant data are those reported in Table II and reference [7]. During the elaboration process, the fibres were held together by molybdenum wire but the original cubic fibre packing was affected by the process. So the fibre packing was not exactly cubic and not exactly hexagonal. The effect of the fibre packing was examined first. Generally the fibre was in compression whereas the matrix was in tension. Inspection of the distribution of TRS obtained by FEM analysis showed a uniform axial and hoop stress field throughout the unit cells with non contacting fibres. The

TABLE IV TRS calculated with a SC thickness equal to 1000 μm using the two different rules of mixtures presented in Section 2.5. The stresses were those at 3 μm of the interface in both materials

		Using ROM 1	Using ROM 2
Stresses in the fibre	Axial	− 192	− 228
	Radial	27	− 96
	Hoop	27	− 96
Stresses in the matrix	Axial	257	166
	Radial	31	− 92
	Hoop	301	191

TABLE V Axial and hoop components of TRS (MPa) determined by FEM analysis for one-dimensional unit cells with uniformly distributed fibres

		Fibre packing arrangement	
		Cubic	Hexagonal
Stresses in the fibre	Axial	− 260	− 290
	Hoop	40	70
Stresses in the matrix	Axial	290	340
	Hoop	330	360

average values of these stress components are given in Table V. Radial TRS depended upon position and direction. Radial TRS profiles are shown as an example in Fig. 19 for a unidirectional composite with cubic packing.

Table V shows that the TRS are not strongly affected by the fibre packing arrangement selected for the analysis. The TRS were generally 20% higher with the hexagonal arrangement. So TRS dependence upon fibre packing arrangement should be regarded as rather small. In this respect, the problem of contacting fibres was examined only for a cubic arrangement. It is worth pointing out that TRS computed for the one-dimensional composites with no contacting fibres compare fairly well with those obtained for the monocomposites with SC. Nevertheless, the one-dimensional composite should be regarded as an assembly of juxtaposed monocomposites with no contacting fibres. However, it is also worth pointing out that TRS computed for the one-dimensional composites highlights a very high level of stress at the free surface of the composite. This phenomenon increased when increasing the number of plies used. This fact has already been reported by several authors [5, 7, 8, 14].

When the distance between two fibres decreased then the TRS varied. The axial stresses were the most affected and it was possible to identify two different areas in the composite: (i) between the fibres, where the level of axial stresses increased and (ii) outside the fibres pack, where the level of axial stress decreased. The hoop stresses were not significantly affected but the same trend was observed for axial stress. Furthermore, the radial stresses varied from positive (tensile) to negative (compressive) values in and outside the fibres pack. It was not possible as in ceramic matrix composites [3] to identify separate positive and negative areas of axial stresses. The incidence of the distance between two fibres is shown in Fig. 20.

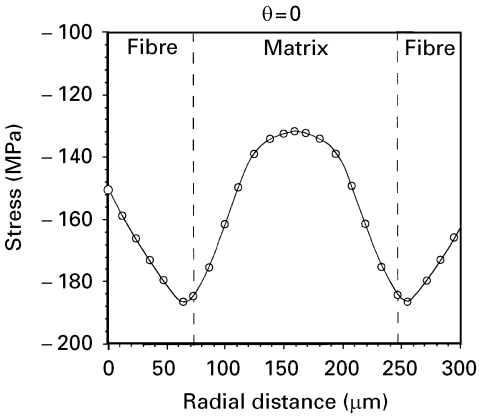

Figure 19 Radial TRS distributions along the fibre radii obtained for a unidirectional composite (cubic fibre packing arrangement). $\theta = 0$ direction was given by the line joining the centres of two neighbouring fibres.

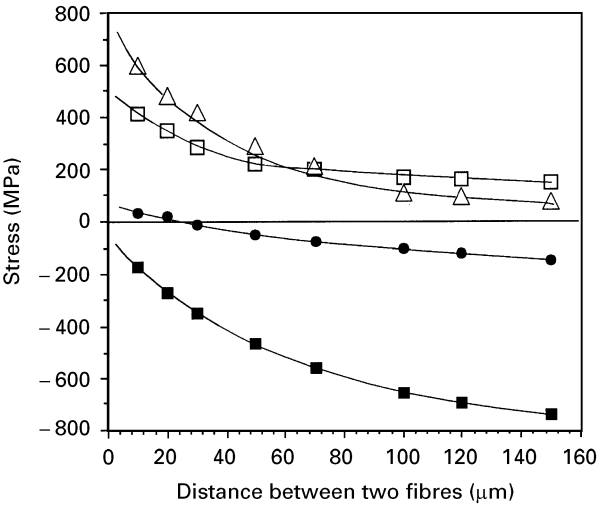

Figure 20 TRS as a function of the distance between two fibres for a cubic fibre packing. The reported stresses were those calculated at 5 μm of the fibre–matrix interface. f, fibre; m, matrix; long, longitudinal; rad, radial; ■ σ_f^{long}; ● σ_f^{rad}; □ σ_m^{long}; △ σ_m^{hoop}.

The high surface stresses were not affected and remained very high. In fact, these results were in good agreement with those obtained and reported in Section 3.1.2 about influence of matrix volume fraction. When the distance between two fibres decreased it meant that the matrix volume fraction between these fibres decreased so that the results obtained were similar when the distance decreased or when the matrix volume fraction decreased. However, while the trends were the same, the data were slightly different and also it was not possible in Section 3.1.2 to predict the axial stress level outside the fibre packing.

3.3. Relaxation of TRS during a fatigue test

In this section the model described in Section 2.4 was used and the thermomechanical data used for both constituents were those reported in Table III and reference [8]. As we did not know the true elastic cyclic limit as a function of the applied stress, we used

an average one in the calculations so that the data obtained as a function of the applied stress could be used only to show and estimate the trends and not to give data to be compared with experimental ones.

Typical results are shown in Figs 21 and 22.

From Fig. 21, the following interesting features should be highlighted:

1. When the applied load increased the relaxation of TRS increased, so the level of TRS in the three directions decreased;
2. The evolution of TRS as a function of applied load was not linear, so when the applied load was close to the maximum yield stress (689.5 MPa by [5]), there was no more variation of the relaxation of TRS.

The minimum stress which it was possible to reach after 5 cycles was about 65% of the initial stress.

From Fig. 22, the following interesting features should be highlighted:

1. The relaxation of axial TRS was very high for the first cycles and later became lower;
2. The relaxation of the hoop TRS was lower than for the axial TRS and it appeared to be a more linear decrease.

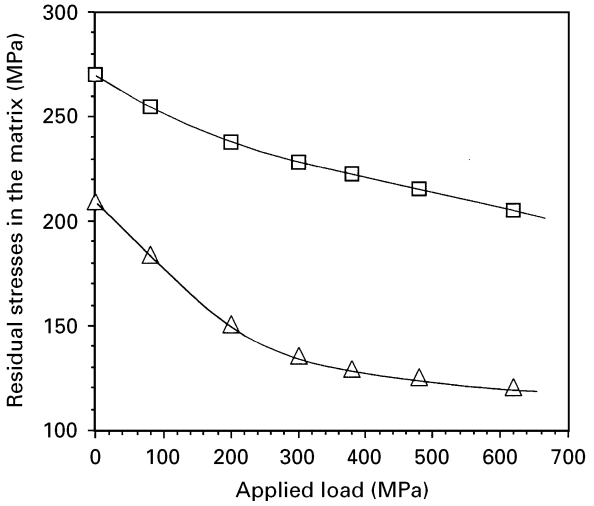

Figure 21 Evolution of TRS after five cycles as a function of applied load. □ σ_m^{long}; △ σ_m^{hoop}.

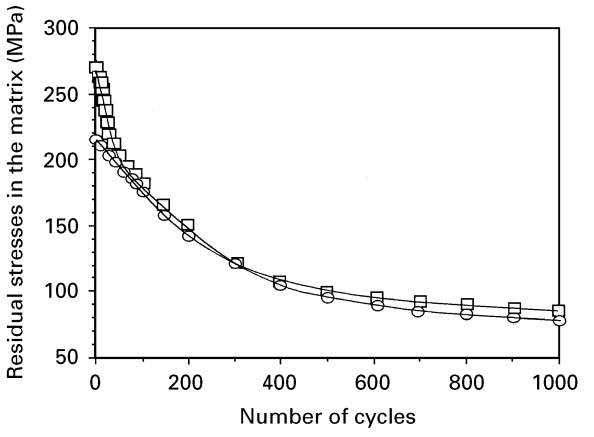

Figure 22 Evolution of TRS during a fatigue test as a function of the number of cycles. □ σ_m^{long}; △ σ_m^{hoop}.

From these results it appears that the relaxation of the TRS is very quick so that, after only 100 cycles more than half of TRS relaxes. Furthermore, the axial stresses, which were assumed to play an important role on mechanical behaviour of the material and especially on fatigue behaviour, were the most quickly relaxed (more than 50% relaxation after only 50 cycles).

After about 1000 cycles no more TRS relaxation occurred and a one-third value of the initial TRS was reached.

4. Conclusions

The residual stress field induced in MMC by cooling down from the processing temperature was evaluated on monocomposites and one-dimensional composites with various fibre packing arrangements. An analytical model was used for the determination of TRS on monocomposites. TRS in monocomposites and one-dimensional composites were then computed using MARC and MENTAT finite element code.

In general, tensile TRS were observed in the matrix of monocomposites, whereas the fibre was in compression.

Calculations for monocomposites showed that the trends for axial and hoop TRS were not affected by the presence of a surrounding composite, whereas the radial stresses could turn tensile. The same observation could be done for one-dimensional composites. In fact, in one-dimensional composites, the TRS computed with no contacting fibres were in excellent agreement with those established for monocomposites with a surrounding composite. The TRS were not significantly affected by the use of a cubic or hexagonal fibre packing arrangement.

Some differences were observed when the distance between two fibres varied. When fibres were closely in contact, higher tensile stresses arose in the inner matrix volumes bounded by neighbouring fibres whereas the periphery was subject to significant lower tensile stresses. On the basis of this result it could be foreseen that cracks will initiate preferentially from the interior of one-dimensional specimens and especially in an area where fibres were close to other ones.

A minimum thickness (in order that the thickness did not affect the TRS calculations) of the surrounding composite of about 500 μm was also determined.

Calculations for monocomposites showed that TRS were not greatly affected by uncertainty in fibre Young's modulus. The TRS were affected to a similar degree by uncertainty in fibre CTE and in matrix Young's modulus. Moreover, increasing fibre CTE led to a decrease of TRS, whereas increasing matrix Young modulus led to an increase of TRS. The matrix CTE uncertainty was the most critical parameter. Thus, the calculated TRS should not be regarded as exact but only the trend could be used when the properties of the matrix (and also to a lesser extent those of the fibre) are not precisely known.

During a fatigue test, relaxation of TRS increased when the number of cycles increased and also when the load increased (but this phenomenon was more

sensitive to the number of cycles than to the applied loading).

More than half of TRS were relaxed after only 100 cycles and the axial stresses were the most quickly relaxed. After about 1000 cycles no more relaxation occurred and the value of TRS reached was about one-third of the initial value.

Acknowledgements

The authors acknowledge the support that they received from the Science and Technology Agency of Japan, through a grant given to J.L.B. They are indebted to K. Gotoh, K. Honda and Y. Yamawaki for fruitful discussion about the finite element model.

References

1. G. E. DIETER, in "Mechanical Metallurgy", 2nd edition, McGraw-Hill, New York (1976), p. 451.
2. P. S. TURNER, *J. Res. Natl. Bur. Stand.* **37** (1946) 239.
3. J. -L. BOBET and J. LAMON, *Acta Metall.* **43** (1995) 2241.
4. *Idem. Mat. Tec.* 92, *Grenoble* (1992) 534.
5. W. S. JOHNSON, S. J. LUBOWINSKI and A. L. HIGHSMITH, in "Thermal and Mechanical Behavior of Metal Matrix and Ceramic Matrix Composites", ASTM STP 1080, edited by J. M. Kennedy, H. H. Moeller and W. S. Johnson (American Society for Testing and Materials, Philadelphia, 1990) p. 193.
6. J. -L. BOBET, Ph.D Thesis n 987, University of Bordeaux (1993).
7. C. A BIGELOW, *J. Comp. Tech. Research*, **15** (1993) 304.
8. J. G. BACKUCKAS, W. S. JOHNSON and C. A. BIGELOW, *J. Engng Mater. and Technol.* **115** (1993) 404.
9. Y. KAGAWA, *Mater. Trans. JIM* **35** (1994) 00.
10. J. ZARKA and J. CASIER, *Mechanics Today* **5** (1979) 93.
11. P. RANGASWAMY, W. C. REVELOS and N. JAYARAMAN, *J. Comp. Tech. Research* **16** (1994) 47.
12. P. RANGASWAMY and N. JAYARAMAN, *Ibid.* **16** (1994) 54.
13. W. D. POLLOCK and W. S. JOHNSON, "Composites Materials: Testing and Design", Vol. 10, ASTM STP 1120, edited by G. G. Grimes (American Society for Testing and Materials, Philadelphia, 1992) p. 175.
14. B. M. HILLEBERRY and W. S. JOHNSON, *J. Comp. Tech. Res.* **14** (1992) 221.
15. Y. MIKATA and M. TAYA, *J. Comp. Mater.* **19** (1985) 554.

Received 9 August 1995
and accepted 10 January 1996